



Deposited via The University of Leeds.

White Rose Research Online URL for this paper:

<https://eprints.whiterose.ac.uk/id/eprint/80313/>

Version: Accepted Version

Article:

Goldobin, DS, Brilliantov, NV, Levesley, J et al. (2014) Non-Fickian diffusion and the accumulation of methane bubbles in deep-water sediments. *European Physical Journal E*, 37 (5). 45. ISSN: 1292-8941

<https://doi.org/10.1140/epje/i2014-14045-x>

Reuse

Items deposited in White Rose Research Online are protected by copyright, with all rights reserved unless indicated otherwise. They may be downloaded and/or printed for private study, or other acts as permitted by national copyright laws. The publisher or other rights holders may allow further reproduction and re-use of the full text version. This is indicated by the licence information on the White Rose Research Online record for the item.

Takedown

If you consider content in White Rose Research Online to be in breach of UK law, please notify us by emailing eprints@whiterose.ac.uk including the URL of the record and the reason for the withdrawal request.

Non-Fickian Diffusion and the Accumulation of Methane Bubbles in Deep-Water Sediments

D. S. Goldobin^{1,3}, N. V. Brilliantov¹, J. Levesley¹, M. A. Lovell², C. A. Rochelle⁴, P. D. Jackson⁴, A. M. Haywood⁵, S. J. Hunter⁵, and J. G. Rees⁴

¹ Department of Mathematics, University of Leicester, Leicester LE1 7RH, UK

² Department of Geology, University of Leicester, Leicester LE1 7RH, UK

³ Institute of Continuous Media Mechanics, UB RAS, Perm 614013, Russia

⁴ British Geological Survey, Keyworth, Nottingham NG12 5GG, UK

⁵ School of Earth and Environment, University of Leeds, Leeds LS2 9JT, UK

June 3, 2014

Abstract. In the absence of fractures, methane bubbles in deep-water sediments can be immovably trapped within a porous matrix by surface tension. The dominant mechanism of transfer of gas mass therefore becomes the diffusion of gas molecules through porewater. The accurate description of this process requires non-Fickian diffusion to be accounted for, including both thermal diffusion and gravitational action. We evaluate the diffusive flux of aqueous methane considering non-Fickian diffusion and predict the existence of extensive bubble mass accumulation zones within deep-water sediments. The limitation on the hydrate deposit capacity is revealed; too weak deposits cannot reach the base of the hydrate stability zone and form any bubbly horizon.

PACS. 66.10.C- Diffusion and thermal diffusion – 47.56.+r Fluid flow through porous media – 91.50.Hc Marine geology: gas and hydrate systems

1 Introduction

The occurrence of methane bubbles within porous water-saturated sediments is widespread around the ocean margins. The gas within them plays an important role in both submarine hazards, such as submarine landslides [1], as well as the formation of resources, such as methane-hydrate deposits [2,3]. The stability of the bubbles has a significant control on the methane flux from the sediments into the ocean-atmosphere system and, thus, can have an impact on the climate change [4,5].

In porous sediments the bubbles are trapped within the matrix pores. Large moving bubbles are unstable, as they split into smaller bubbles during migration [6,7], and smaller bubbles are trapped by pore-throats or by surface tension forces. The minimum pore throat diameter l required to trap a small bubble, when there is no strong pumping of the fluid through the porous matrix, can be calculated. The surface tension forces σl (σ is the surface tension) should overwhelm the buoyancy force $\rho g l^3$ (ρ is the density, g is the gravity), i.e., $l < \sqrt{\sigma/\rho g}$. For gas-water systems, one finds, $l < 2.7$ mm. Making allowance for the inhomogeneity of pores and the geometry of contacts, one should decrease this estimate to $l \approx 1$ mm, which still suggests trapping even for sands. For a soft mud, mechanics of bubbles and porous matrix can be different [8] and is not considered here.

As bubbles are trapped, and in the absence of significant groundwater movement transporting dissolved methane, the dominant mechanism of methane mass transfer in deep-water sediment is by diffusion of methane through porewater, controlled by (i) the methane saturation of the aqueous solution throughout the sediment volume, and (ii) non-Fickian diffusion laws. The latter pertain to two processes: firstly, the geothermal gradient causes thermal diffusion (the Soret effect [9]), where the temperature gradient induces solute flux (as recognized in several fields, e.g. [10]); and secondly, the impact of gravity on dissolved molecules [11]. These non-Fickian contributions to the diffusive flux mean that the solute flux cannot solely be determined by the gradient of the solute concentration.

Currently non-Fickian diffusion is rarely considered in the modelling of deep-water sediment systems; in gas hydrate modelling [2,3,12–16], only Fickian diffusion is accounted for. However, we suggest that non-Fickian processes are important; in particular, they may cause methane to migrate against the direction of the steepest decrease of concentration under certain conditions. Importance of non-Fickian diffusion was also demonstrated for the salinity transport in hydrate-bearing sediments [17]. Unfortunately, the experimental value of the thermal diffusion coefficient for the aqueous methane solution is un-

known and can only be roughly assessed theoretically. Therefore, we treat it as a free parameter in our investigation. This uncertainty also justifies the fact that prior numerical modelling work did not include non-Fickian processes.

In researching the horizontal through-flow of water and vertical aqueous oxygen transport in porous bubble-bearing sediments, Donaldson et al. [18] considered the hydrodynamic dispersion (*or* “turbulent diffusion” [19]), caused by water transport through irregular pore channels, as a transport mechanism and reasonably neglected the molecular diffusion. Indeed, the turbulent diffusion plays a significant role in vertical dissolved gas transport near the earth’s surface. However, it becomes insignificant away from the sediment-water interface in deep-water sediments, where vertical and horizontal displacements of water are comparable. Here it is significantly smaller than molecular diffusion—even in sandy sediments.

In the present study we consider the diffusive migration of methane in sea-floor sediments where water is saturated with methane, and some methane is gaseous (forming bubbles; see the sketch in Fig. 1a). In deep-water sediments the bubbly zone is overlaid by the methane hydrate stability zone, where non-dissolved methane forms not gaseous bubbles but hydrate, which is included in our treatment as well.

2 Transport processes in sediments

On the field scale, deep-water sediments are typically much more uniform horizontally rather than vertically. Consequently, we consider a system that is uniform horizontally. The depth below the water-sediment interface is measured by the z -coordinate (Fig. 1).

2.1 Diffusion in non-isothermal aqueous solutions

Under non-isothermal conditions the diffusive flux of solute mass is governed by the law (cf [20,31])

$$\mathbf{J}_{\text{diff}} = -\chi\phi\rho_f D \omega \left[\frac{\nabla\omega}{\omega} + \alpha \frac{\nabla T}{T} - \frac{\tilde{M}\mathbf{g}}{RT} \right]. \quad (1)$$

Here ω is the mass fraction of the solute in the solvent, D is the solute molecular diffusion coefficient, ϕ is the porosity of the solid matrix, χ is the tortuosity factor featuring the pore geometry, ρ_f is the fluid density. The first term describes the “ordinary” Fickian diffusion, $\mathbf{J}_{\text{Fick}} = -\chi\phi\rho_f D \nabla\omega$. The second term represents the thermal diffusion effect appearing in non-isothermal systems, where temperature inhomogeneity causes a solute flux. The strength of the thermal diffusion effect is characterized by the thermal diffusion factor α (the conventional Soret *or* separation coefficient $S_T = \alpha/T$). The third term describes the action of gravity on solute molecules; $R = 8.31 \text{ J}/(\text{mol K})$ is the universal gas constant, $\tilde{M} = M^g - N_1 M^{\text{host}}$, M^g and M^{host} are the molar

masses of the solute and solvent, respectively, and N_1 is the number of solvent molecules in the volume occupied by one solute molecule in the solution. The value of N_1 can be precisely derived for $\text{CH}_4\text{-H}_2\text{O}$ systems from the dependence of the solution density on its concentration [21]; one obtains $N_1 = 2.23$ and $\tilde{M} = -24.3 \text{ g/mol}$.

When the liquid is saturated with gas bubbles, the concentration of solute in solvent equals the solubility, $\omega = \omega^{(0)}$, throughout the liquid volume in the bubble-bearing zone because the bubbles are in local thermodynamic equilibrium with the solution. Thus, the solute flux depends merely on the temperature and pressure fields, $T(z)$ and $P(z)$, and the solution concentration is not a free variable, $\omega(z) = \omega^{(0)}(T(z), P(z))$. At high pressure and low enough temperature, the hydrate form is more thermodynamically preferable for methane than the gaseous form. The hydrate zone can overlie the bubbly-bearing zone (Fig. 1). In the presence of hydrate the solution concentration equals the solubility at equilibrium with hydrate. For the calculation of the solubility (in bubbly and hydrate zones), half-empiric models developed in [22,23] are employed.

Generally, the thermal diffusion factor α and N_1 depend on solution concentration and temperature. Solutions of weakly soluble substances (such as methane in water) are close to the infinitely dilute solution limit, i.e., in our case the values of parameters should be taken for vanishing concentration. Variation of temperature across the sediment system rarely exceeds 20 K, which is small compared to the absolute value of temperature ($\sim 300 \text{ K}$); therefore, we neglect the dependence on temperature for those values which depend polynomially (the thermal diffusion factor α , water density, and N_1), and account for this dependence when it is exponential (molecular diffusion coefficient D and solubility). An additional reason to ignore the temperature dependence of α at the current stage of our consideration of the problem is the lack of knowledge on it for aqueous solutions of methane in the literature.

2.2 Pressure and temperature

The solubility profiles and thus transport processes depend on the pressure and temperature profiles. The system is essentially characterized by the hydrostatic pressure P and geothermal temperature gradient G . Although the role of porosity nonuniformity for the geothermal gradient was demonstrated in [24], we follow the conventional approximation of a linear temperature profile [2,16,15]. Therefore,

$$P(z) = P_0 + \rho_f g(z + H), \quad T(z) = T_{\text{sf}} + Gz, \quad (2)$$

where P_0 is the atmospheric pressure, H is the depth of the water body above the bubble-bearing porous sediments, and T_{sf} is the temperature at the sediment-water interface.

2.3 Sediment compaction and transport processes

The sedimentation process and the weight of the above-laying sediments result in a non-uniform porosity profile and a non-uniform velocity of the downward sediment motion. The sediment porosity is typically adopted in the form $\phi(z) = \phi_0 \exp(-z/L)$ [2,15], and the resulting sediment velocity is [2]

$$v_s(z) = \frac{1 - \phi_0}{1 - \phi(z)} v_s(0), \quad (3)$$

where $v_s(0)$ is the sedimentation rate.

The sedimentation and compaction processes create an ascending filtration flux of water through the sediments. The net water mass flux $\mathbf{J}_{\text{H}_2\text{O}}$ is contributed by the filtration flux \mathbf{u}_f and by the water transport in hydrate, which moves with sediments;

$$\mathbf{J}_{\text{H}_2\text{O}} = \rho_f \mathbf{u}_f + K_{\text{H}_2\text{O}} \rho_h h \phi \mathbf{v}_s, \quad (4)$$

where ρ_h is the hydrate density, $K_{\text{H}_2\text{O}} \approx 0.866$ is the mass fraction of H_2O in methane hydrate, and h is the volumetric fraction of hydrate in pores *or* hydrate saturation.

Whilst the volumetric fraction of bubbles (*or* gas saturation) in pores, say b , is vanishingly small, bubbles are immovably trapped in pores and move with sediments [2, 15,25]. However, transport processes in the system can result in a gas saturation which exceeds the critical value b_{cr} . When the critical saturation is exceeded, gas leakage occurs.

The net methane mass flux \mathbf{J}_{CH_4} is contributed by the ascending filtration flux of aqueous solution, the motion of gas bubbles and/or hydrate with sediments, and molecular diffusion in aqueous solution. In the absence of gas leakage, it reads

$$\mathbf{J}_{\text{CH}_4} = \rho_f \omega \mathbf{u}_f + (K_{\text{CH}_4} \rho_h h + \rho_b b) \phi \mathbf{v}_s - \chi(1 - h - b) \phi \rho_f D \omega (\nabla \ln \omega + \beta \nabla \ln T), \quad (5)$$

where the tortuosity factor is assumed $\chi = 0.75$ [15], $K_{\text{CH}_4} = 1 - K_{\text{H}_2\text{O}}$ is the mass fraction of CH_4 in hydrate, and

$$\beta = \alpha - \frac{\tilde{M}g}{RG}. \quad (6)$$

Eq. (5) with $\beta = 0$ corresponds to the Fickian diffusion law, $\mathbf{J}_{\text{Fick}} = -\chi \phi \rho_f D \nabla \omega$, and β characterizes the *strength of non-Fickian part of the solute flux*. As the value of α is unknown, β is treated as a free parameter in our study. In our model, the zones of hydrate and gas bubbles do not overlap; either b or h can be non-zero at a given location.

While the diffusion coefficient D of methane in water is nearly insensitive to variations of pressure in the range from 1 to 200 atm [26], its dependence on temperature is not to be neglected as the temperature change from 273 K to 323 K causes the diffusivity increase by factor 4. The formula $D(T) = D_0(T/T_0) \exp[B/(T + \tau) - B/(T_0 + \tau)]$ with $D_0 = 7.38 \cdot 10^{-10} \text{ m}^2/\text{s}$, $T_0 = 273 \text{ K}$, $B = 212 \text{ K}$, $\tau = 71.5 \text{ K}$ well fits experimental data summarized by [26].

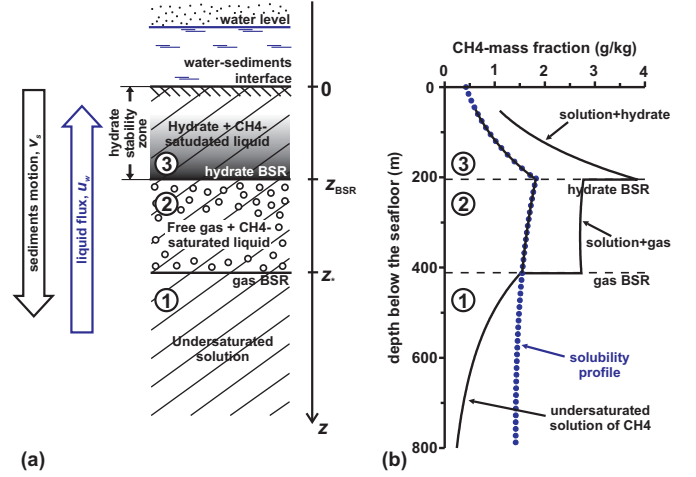


Fig. 1. (a): Sketch of bubble-bearing marine sediments with a hydrate zone (3) overlaying the bubbly zone (2). (b): The aqueous methane solubility profile is plotted with the dotted blue curve for water-body depth $H = 1.5 \text{ km}$ and parameters specified in Tab. 1, which correspond to the west Svalbard continental slope [15]. Black solid line plots the net mass fraction of methane in pores—gaseous methane or methane in hydrate are added to the mass in the aqueous solution—for a time-independent state and $\beta = 2.13$ (i.e., $\alpha = 1.8$), see Eqs. (7)–(9).

In the present work we do not consider details of the process of methane generation from the organic part of sediments, assuming that it occurs in the upper part of sediments and methane is simply present at certain depth of about 100 – 200 m below the water-sediment interface (cf [15]).

3 Results

Both the numerical modelling with finite difference method and analytical treatment were performed. The results of numerical simulation (also including different gas leakage models) are in agreement with the analytical theory (as can be later seen from Fig. 2d). It is convenient to start the presentation of results with time-independent solutions to the problem.

3.1 No-leakage time-independent states

Three zones with different transport features can be distinguished (see Fig. 1):

- (1) the lowermost zone of undersaturated aqueous solution of methane without gas bubbles, $z > z_*$,
- (2) the zone of saturated solution bearing gas bubbles, $z_{\text{BSR}} < z < z_*$, and
- (3) the lower part of hydrate stability zone (HSZ) with saturated solution and hydrate, $z < z_{\text{BSR}}$.

In the lower part of HSZ we consider, no process of conversion of organic sediments into methane occurs; we assume the conversion to be finished above this zone. In

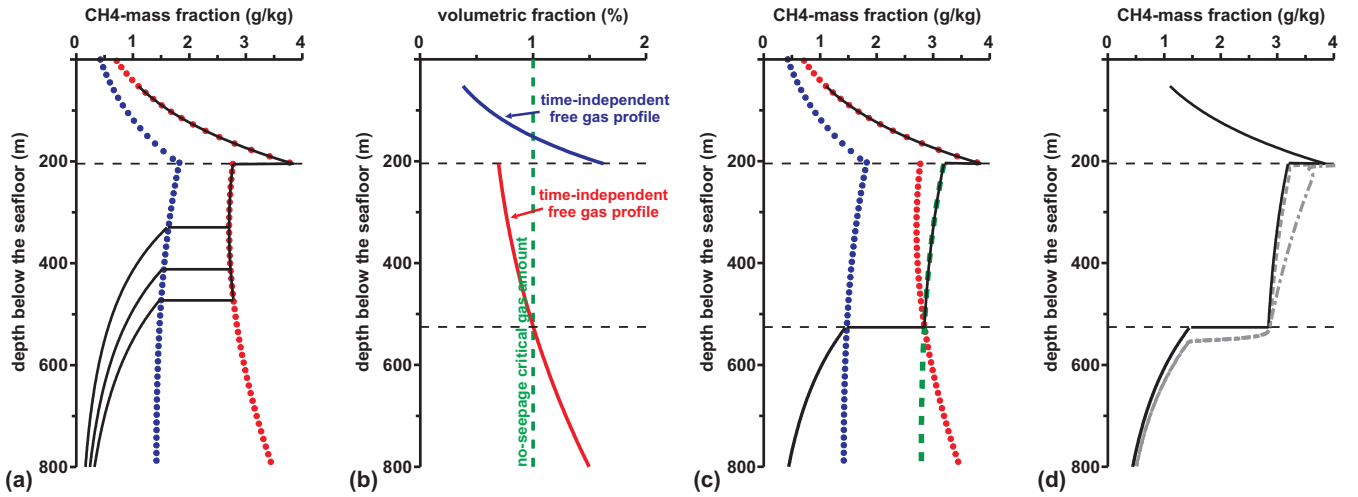


Fig. 2. Methane profiles for the parameter set specified in Tab. 1, $H = 1.5$ km and $\alpha = 0$. (a): Time-independent methane mass profiles (cf Fig. 1b). (b): Volumetric fraction in pores (saturation) of hydrate and methane for time-independent states is compared to the critical gas saturation (green dashed line). (c): Steady methane mass profile with critical gas saturation at the bubbly zone. (d): Analytical solution profile (black solid line), and numerically calculated steady profiles in the free gas zone with the sediment permeability 10^{-12} m² (gray dashed line) and 10^{-13} m² (gray dash-dotted line).

Fig. 1b, one can see a sample profile of the net mass fraction of methane in pores composed of dissolved methane and methane in hydrate or gas bubbles.

At the time-independent state, neither the hydrate distribution nor the free-gas one change with time, which requires the methane mass flux (5) to be uniform along the sediment column. As we do not consider methane influx from deep massifs, i.e., methane mass flux is zero deep in sediments, this uniform flux should be zero everywhere. The water flux (4) is uniform, $J_{\text{H}_2\text{O}} = \rho_f u_{f0}$, where u_{f0} is the filtration velocity below HSZ (cf [2]).

For zero methane flux and given water flux, one can find the solution concentration in zone (1);

$$\omega_1(z) = \omega_1(z_*) \left[\frac{T(z_*)}{T(z)} \right]^\beta \exp \left[\int_{z_*}^z \frac{u_{f0} dz_1}{\chi \phi(z_1) D(z_1)} \right]. \quad (7)$$

In zone (2), the solute concentration equals the solubility, $\omega_2(z) = \omega_2^{(0)}(z)$, and, in the absence of leakage, gas saturation

$$b = \frac{\rho_f \omega_2^{(0)}}{\rho_b v_s} \left(-\frac{u_{f0}}{\phi} + \chi D \frac{d}{dz} \ln(\omega_2^{(0)} T^\beta) \right). \quad (8)$$

Table 1. Geophysical properties characteristic for the west Svalbard continental slope [15]

	parameter	value
T_{sf}	seafloor temperature	-0.9°C
G	geothermal gradient	$86.5^\circ\text{C}/\text{km}$
L	e -folding depth of porosity	1053 m
u_{f0}	fluid filtration velocity	-0.1 mm/year
$v_s(0)$	sedimentation rate	0.5 mm/year
χ	tortuosity factor	0.75

In zone (3), the solute concentration equals the solubility, $\omega_3(z) = \omega_3^{(0)}(z)$, and hydrate saturation

$$h = \frac{\rho_f \omega_3^{(0)}}{K_{\text{CH}_4} \rho_h v_s} \left(-\frac{u_{f0}}{\phi} + \chi D \frac{d}{dz} \ln(\omega_3^{(0)} T^\beta) \right). \quad (9)$$

(Eqs. (8) and (9) are derived from Eqs. (4) and (5) for small h and b .) In Fig. 1b the time-independent state is plotted for $\beta = 0$, the graphs for different β are qualitatively similar. Gas saturation b immediately above the lower boundary of the bubbly zone is finite and enough for the formation of the second bottom simulating reflector of seismic waves, which is not associated with hydrate.

3.2 Evolution of the bubbly zone and persistence of marine hydrate deposits

For a time-independent state determined by Eqs. (7)–(9) the position of the boundary between the bubbly zone and the zone of undersaturated solution is not imposed; all three profile plotted is Fig. 2a satisfy the equations. Now let us consider small deviation from these profiles.

When hydrate saturation h at the base of HSZ is smaller than that in the time-independent state, upward methane flux appears. Indeed, the diffusion flux is the same as in the time-independent state, because it is controlled by the solubility profile, while we have strictly downward transfer of hydrate with sediments, and this transfer is diminished in comparison to the transfer in the time-independent state. In the time-independent state these two fluxes are balanced to zero net flux, while with the deficiency of hydrate we have the deficiency of downward flux and thus the net flux is upward. An upward net flux of methane results in depletion of methane deep in sediments and gradual retreat of the bubbly zone. After some period of time the bubbly zone disappears and,

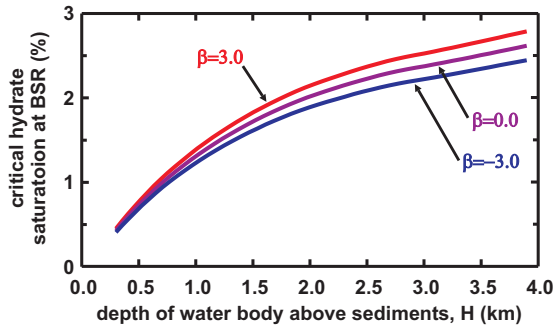


Fig. 3. Minimal hydrate saturation (volumetric fraction in pores) at the base of the hydrate stability zone, which is required for the hydrate deposit to be persistent, is plotted vs the water-body depth H for parameters specified in Tab. 1.

moreover, hydrate zone retreats from the base of HSZ to the area of methane generation from sediments. In this case one observes HSZ with undersaturated aqueous solution and no hydrate at the base of it and no bubbly zone; this has been reported to be widespread in nature [27]. Thus, one can see that the hydrate deposit cannot be too weak, otherwise it is not persistent. In Fig. 3 the minimal hydrate saturation is plotted as a function of the water-body depth; this value is also affected by the non-Fickian drift strength β , for a larger β a stronger deposit is required.

When the hydrate saturation at the base of HSZ exceeds the critical hydrate saturation, one observes an opposite situation: a downward net flux of methane and a bubbly zone gradually advancing into deep sediments. However, the advance of the bubbly zone is not unbounded. In Fig. 2b, one can see that for time-independent states the gas saturation increases with depth and at certain depth, z_* , exceeds the critical gas saturation. The critical gas saturation, above which gas leakage starts, depends on many factors, including the pore geometry and the solid matrix material [25], and the rate of gas release from the solution (for discussion see [15]). The critical gas saturation b_{cr} specific for different porous massifs is about 1% (e.g., see review in [15]), and we adopt this value for our analysis. Leakage is a hydrodynamical transport and as such is much more efficient than the molecular diffusion transport or the motion with sediments. Therefore, any significant excess of gas saturation over the critical value results in a mass flux which cannot be balanced by molecular diffusion or sedimentation, and, on the time scales of the hydrate deposit formation, gas saturation can be only under- or nearly-critical. The bubbly zone cannot advance deeper, as a larger gas saturation is required to have a downward methane transfer below depth z_* . Leaking gas is accumulated just above the leakage zone until the critical saturation is reached there. Then leakage zone extends, and finally entire bubbly zone becomes the leakage zone with gas saturation slightly exceeding the critical saturation, as shown in Fig. 2c. Hence, for persistent hydrate deposits ($h > h_{cr}$) one can observe the formation of extensive bubbly zone with critical gas saturation; the

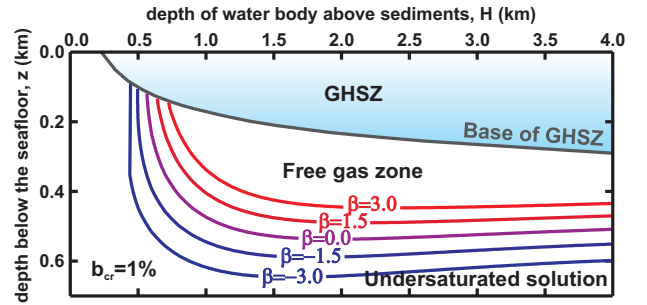


Fig. 4. The bubbly zone is confined between the base of the hydrate stability zone (HSZ) and the gas bottom simulating reflector, which is plotted in different colors for different values of the non-Fickian drift strength β and critical gas saturation $b_{cr} = 1\%$. The parameter set is specified in Tab. 1 and corresponds to the west Svalbard continental slope [15].

lower boundary z_* of this zone is determined by condition

$$\frac{\rho_f \omega_2^{(0)}}{\rho_b v_s} \left(-\frac{u_{f0}}{\phi} + \chi D \frac{d}{dz} \ln(\omega_2^{(0)} T^\beta) \right) \Big|_{z=z_*} = b_{cr}. \quad (10)$$

In Fig. 2d, one can compare the analytical time-independent profile to the results of numerical simulation with a comprehensive account of processes: the rate of methane generation by anaerobic bacteria

$$Q(z) = A_0 \lambda [1 - \phi(z)] \exp \left(-\lambda \int_0^z \frac{dz_1}{v_s(z_1)} \right)$$

with $\lambda = 5 \cdot 10^{-13} \text{ s}^{-1}$ and $A_0 = 14.4 \text{ kg/m}^3$ (cf [2]) and the gas leakage within the bubbly zone with relative permeability for the gas phase $k_g = b(b - b_{cr} + |b - b_{cr}|)/2$ [28]. The numerically calculated profile slightly deviates from the analytical one for realistic sediment permeability and this deviation remains non-large even for as small permeability as 10^{-13} m^2 . Noteworthy, the base of the free-gas zone remains unshifted even for small permeability.

In numerical simulation the described evolution was observed with different leakage laws, which may strongly vary from system to system (e.g. [25]), and realistic values of massif permeability. As explained and demonstrated in Fig. 2d, the bubbly zone is tolerant to specific features of the leakage law with given b_{cr} ; realistic model parameters can only change the small excess of the gas saturation over the critical value. In our analytical theory we do not discuss the narrow hydrate-gas recycling zone immediately below HSZ, where gas saturation may significantly exceed the critical saturation. Features of this zone depend on the leakage model which is highly uncertain without thorough knowledge of the massif properties and is site-specific.

In Fig. 4, one can see that the location of the extensive free-gas (bubbly) zone is affected by the non-Fickian drift strength β . Moreover, the minimal depth of the water body above sediments needed for the extensive bubbly zone to appear is also controlled by β . An extensive bubbly zone is not possible below HSZ beneath shallow water bodies because the time-independent state requires gas saturation higher than the critical saturation and cannot

be maintained because of gas leakage. It is noteworthy that, due to hydrate–gas recycling, a narrow bubbly layer immediately below HSZ will be still presented wherever hydrate is present at the base of HSZ.

3.3 Importance and uncertainties

The behavior described is considerably influenced by the non-Fickian drift of methane. We suggest that the Fickian diffusion law, which has been adopted in [2] and its successors and corresponds to $\beta = 0$, should be modified.

The unresolved issue here is the specific value of β for methane. The authors are not aware of experimental data on thermal diffusion of methane in water, though there are a lot of experimental studies on the thermal diffusion of methane in mixtures of hydrocarbons (e.g. [29]). Theoretical studies (e.g. [30]) provide formulae for calculation of the thermal diffusion factor from inter-molecular potentials which are poorly established for water because of hydrogen bonds. We can only calculate $\tilde{M}g/RG = -0.331$ (for $G = 86.5$ K/km) and use a rough conjecture that one can expect $\alpha \approx 1.8$ [31]. Hence, $\beta \approx -2.13$ can be expected for aqueous solutions with geothermal gradient $G = 86.5$ K/km.

4 Conclusion

We have theoretically explored the process of diffusive migration of aqueous methane in the presence of bubbles, when they are immovably trapped by a porous matrix—as occurs commonly in seafloor sediments, swamps, or terrestrial aquifers. The effect of temperature inhomogeneity across the system (geothermal gradient) and gravitational force have been accounted for.

Non-Fickian corrections—thermal diffusion and gravitational segregation—appear to play an important role in the migration of methane in sediments in deep-water settings. The positive thermal diffusion effect ($\alpha > 0$, cf Eq. (6)) and the gravitations segregation of methane in water make negative contribution to β , and, therefore, they assist the formation of an extensive methane gas accumulation zone in the upper part of the sediment column under deep water bodies. For instance, Fig. 4 illustrates that, for conditions of the west Svalbard continental slope [15], non-Fickian diffusion can either extend ($\beta < 0$) or shrink ($\beta > 0$) the zone of methane gas accumulation.

Remarkably, hydrate deposits with too small hydrate saturation at the base of the hydrate stability zone should suffer diffusive depletion and retreat from the base of HSZ to the region of methane generation from sediments or completely disappear. This explains why some natural hydrate deposits are reported to possess no hydrate and no bottom simulating reflector at the base of HSZ. The positive thermal diffusion effect and gravitational segregation, both resulting in negative β , decrease the minimally required hydrate saturation, as can be seen in Fig. 3.

Unfortunately, we cannot determine precise values for the thermal diffusion factor of aqueous solutions of

methane from the literature, and can only rely on theoretical predictions (e.g. [30,31]), to estimate their values, as we do here. Our findings highlight the necessity of experimental determinations of the thermal diffusion factor for aqueous methane solutions.

The work has been supported by NERC (NE/F021941/1). DSG acknowledges the financial support by the Government of Perm Region (Contract C-26/212). This paper is published with the permission of the Director of the British Geological Survey.

References

1. R. E. Kayen and H. J. Lee, *Pleistocene slope instability of gas hydrate-laden sediment on the Beaufort Sea margin*, Marine Geotechnology **10**, 125–141 (1991).
2. M. K. Davie and B. A. Buffett, *A numerical model for the formation of gas hydrate below the seafloor*, J. Geophys. Res. **106**, 497–514 (2001).
3. M. K. Davie and B. A. Buffett, *Sources of methane for marine gas hydrate: inferences from a comparison of observations and numerical models*, Earth Planet. Sci. Lett. **206**, 51–63 (2003).
4. D. Archer, *Methane hydrate stability and anthropogenic climate change*, Biogeosciences **4**, 521–544 (2007).
5. S. J. Hunter, D. S. Goldobin, A. M. Haywood, A. Ridgwell and J. G. Rees, *Sensitivity of the global submarine hydrate inventory to scenarios of future climate change*, Earth Planet. Sci. Lett. **367**, 105–115 (2013).
6. D. V. Lyubimov, S. Shklyayev, T. P. Lyubimova and O. Zikanov, *Instability of a drop moving in a Brinkman porous medium*, Phys. Fluids **21**, 014105 (2009).
7. M. A. Barry, B. P. Boudreau, B. D. Johnson and A. H. Reed, *First-order description of the mechanical fracture behavior of fine-grained surficial marine sediments during gas bubble growth*, J. Geophys. Res. **115**, F04029 (2010).
8. C. K. Algar, B. P. Boudreau and M. A. Barry, *Initial rise of bubbles in cohesive sediments by a process of viscoelastic fracture*, J. Geophys. Res. **116**, B04207 (2011).
9. C. Soret, *Sur l'état d'équilibre que prend, au point de vue de sa concentration, une dissolution saaline primitivement homogène, dont deux parties sont portées à des températures différentes*, Archives des Sciences Physiques et Naturelles de Genève **2**, 48–61 (1879).
10. J. Richter, *Evidence for significance of other-than-normal diffusion transport in soil gas exchange*, Geoderma **8**, 95–101 (1972).
11. G. Galliéro and F. Montel, *Nonisothermal gravitational segregation by molecular dynamics simulations*, Phys. Rev. E **78**, 041203 (2008).
12. M. E. Torres, K. Wallmann, A. M. Tréhu, G. Bohrmann, W. S. Borowski and H. Tomaru, *Gas hydrate growth, methane transport, and chloride enrichment at the southern summit of Hydrate Ridge, Cascadia margin off Oregon*, Earth Planet. Sci. Lett. **226**, 225–241 (2004).
13. B. Buffett and D. Archer, *Global inventory of methane clathrate: sensitivity to changes in the deep ocean*, Earth Planet. Sci. Lett. **227**, 185–199 (2004).
14. J. B. Klauda and S. I. Sandler, *Global Distribution of Methane Hydrate in Ocean Sediment*, Energy Fuels **19**, 459–470 (2005).

15. R. R. Haacke, G. K. Westbrook and M. S. Riley, *Controls on the formation and stability of gas hydrate-related bottom-simulating reflectors (BSRs): A case study from the west Svalbard continental slope*, *J. Geophys. Res.* **113**, B05104 (2008).
16. S. K. Garg, J. W. Pritchett, A. Katoh, K. Baba and T. Fujii, *A mathematical model for the formation and dissociation of methane hydrates in the marine environment*, *J. Geophys. Res.* **113**, B01201 (2008).
17. D. S. Goldobin, *Non-Fickian diffusion affects the relation between the salinity and hydrate capacity profiles in marine sediments*, *Comptes Rendus Mecanique* **341**, 386–392 (2013).
18. J. H. Donaldson, J. D. Istok, M. D. Humphrey, K. T. O'Reilly, C. A. Hawelka and D. H. Mohr, *Development and testing of a kinetic model for oxygen transport in porous media in the presence of trapped gas*, *Ground Water* **35**, 270–279 (1997).
19. R. A. Bernard and R. H. Wilhelm, *Turbulent diffusion in fixed beds of packed solids*, *Chem. Eng. Prog.* **46**, 233–244 (1950).
20. R. B. Bird, W. E. Stewart and E. N. Lightfoot, *Transport Phenomena* (Wiley, 2007).
21. L. Hnedkovský, R. H. Wood and V. Majer, *Volumes of aqueous solutions of CH₄, CO₂, H₂S and NH₃ at temperatures from 298.15 K to 705 K and pressures to 35 MPa*, *J. Chem. Thermodyn.* **28**, 125–142 (1996).
22. Z. Duan and S. Mao, *A thermodynamic model for calculating methane solubility, density and gas phase composition of methane-bearing aqueous fluids from 273 to 523 K and from 1 to 2000 bar*, *Geochim. Cosmochim. Acta* **70**, 3369–3386 (2006).
23. R. Sun and Z. Duan, *An accurate model to predict the thermodynamic stability of methane hydrate and methane solubility in marine environments*, *Chem. Geol.* **244**, 248–262 (2007).
24. D. S. Goldobin, *Scaling of transport coefficients of porous media under compaction*, *Europhys. Lett.* **95**, 64004 (2011).
25. S. Abaci, J. Edwards and B. Whittaker, *Relative permeability measurements for two phase flow in unconsolidated sands*, *Mine Water Environ.* **11**, 11–26 (1992).
26. W. Sachs, *The diffusional transport of methane in liquid water: method and result of experimental investigation at elevated pressure*, *J. Pet. Sci. Eng.* **21**, 153–164 (1998).
27. C. K. Paull, R. Matsumoto, P. J. Wallace and W. P. Dillon (Eds.), *Proceedings of the Ocean Drilling Program, in: Scientific Results, vol. 164* (Ocean Drilling Program, College Station, TX, 2000).
28. G. Mavko, T. Mukerji and J. Dvorkin, *The Rock Physics Handbook* (Cambridge University Press, 2009).
29. S. Wiegand, *Thermal diffusion in liquid mixtures and polymer solutions*, *J. Phys.: Condens. Matter* **16**, R357–R379 (2004).
30. S. N. Semenov, *Statistical thermodynamic expression for the Soret coefficient*, *Europhys. Lett.* **90**, 56002 (2010).
31. D. S. Goldobin and N. V. Brilliantov, *Diffusive migration of mass in bubbly media*, *Phys. Rev. E* **84**, 056328 (2011).